mark the richness of life's history and constitute the only scale of evolution directly observable in our own historic time. The *Cerion* fossil record thus supplies an empirical bridge between these two crucial scales of evolution.

REFERENCES AND NOTES

1. D. S. Woodruff and S. J. Gould, *Evolution* **41**, 1022 (1987); P. Bartsch, *Carnegie Inst. Washington Yearbk.* **20**, 198 (1922); *ibid.* **30**, 373 (1931).
2. N. H. Barton and G. M. Hewitt, *Annu. Rev. Ecol. Syst.* **16**, 113 (1985).
3. J. M. Szymura, in *Hybrid Zones and the Evolutionary Process*, R. G. Harrison, Ed. (Oxford Univ. Press, New York, 1993), pp. 261–289.
4. G. M. Hewitt, *ibid.*, pp. 140–164.
5. S. J. Gould and D. S. Woodruff, *Biol. J. Linn. Soc.* **40**, 67 (1990).
6. "Area effects," as originally defined by A. J. Cain and J. D. Currey [*Philos. Trans. R. Soc. London* **246**, 1 (1963)], occur in geographic regions housing distinctive local populations of a species (in an area larger than that of a panmictic population) where sharp borders separate the population from other distinctive populations of the species but where no evident feature of climate, habitat, or ecology correlates with the sharp change in phenotype. This phenomenon is common in land snails and has generated a large literature, reviewed in (*5*).
7. S. J. Gould, *Paleobiology* **10**, 172 (1984).
8. After cleaning and hydrolysis (in 6 N HCl at 100°C for 20 hours), samples were desalted with HF and analyzed by high-pressure liquid chromatography, with the use of postcolumn *o*-phthaldialdehyde derivatization [P. E. Hare, P. A. St. John, M. H. Engel, in *Chemistry and Biochemistry of the Amino Acids*, G. C. Barrett, Ed. (Chapman & Hall, London, 1985), p. 415]. Peak area ratios were calibrated against a standard A/I mixture. Errors averaged ±4% of the A/I value.
9. G. A. Goodfriend, *Radiocarbon* **31**, 1041 (1989); ——— and R. M. Mitterer, *Geol. Soc. Am. Bull.* **105**, 18 (1993); G. A. Goodfriend, R. A. D. Cameron, L. M. Cook, *J. Biogeogr.* **21**, 309 (1994); G. A. Goodfriend and D. J. Stanley, *Mar. Geol.* **129**, 271 (1996).
10. G. A. Goodfriend and J. J. Stipp, *Geology* **11**, 575 (1983).
11. A. A. Burchuladze *et al.*, *Radiocarbon* **31**, 771 (1989).
12. M. Stuiver and P. J. Reimer, *ibid.* **35**, 215 (1993).
13. S. J. Gould and D. S. Woodruff, *Bull. Am. Mus. Nat. Hist.* **182**, 389 (1986).
14. S. J. Gould, *Evolution* **43**, 516 (1989).
15. G. A. Goodfriend, *Radiocarbon* **29**, 159 (1987).
16. M. Stuiver and G. W. Pearson, *ibid.* **28**, 805 (1986).
17. Laboratory facilities were provided by P. E. Hare, and conventional radiocarbon dates, by I. Carmi. We thank B. Robinson for making measurements and performing biometrical analyses. R. Herschler of the U.S. National Museum of Natural History provided prebomb *Cerion* for radiocarbon analysis. We thank D. S. Woodruff for his role in the fieldwork.

12 September 1996; accepted 24 October 1996

Nanocapillarity and Chemistry in Carbon Nanotubes

D. Ugarte,* A. Châtelain, W. A. de Heer

Open carbon nanotubes were filled with molten silver nitrate by capillary forces. Only those tubes with inner diameters of 4 nanometers or more were filled, suggesting a capillarity size dependence as a result of the lowering of the nanotube-salt interface energy with increasing curvature of the nanotube walls. Nanotube cavities should also be less chemically reactive than graphite and may serve as nanosize test tubes. This property has been illustrated by monitoring the decomposition of silver nitrate within nanotubes in situ in an electron microscope, which produced chains of silver nanobeads separated by high-pressure gas pockets.

The nanoscale cavities of fullerenes (*1*) and nanotubes (*2*) may be used for generating encapsulated compounds or elongated nanostructures. Early attempts to fill fullerene-related materials were based on the electric arc method, in which graphite electrodes were impregnated with the filling material (*3–5*). These experiments led to the discovery of a variety of filled graphitic structures (*6–8*); however, the abundances of filled structures were very low and their production was difficult to control. Alternatively, nanotube production and filling procedures can be separated by using efficient nanotube production methods (*9*) and by utilizing capillary forces (*10–13*) for filling them. Dujardin *et al.* (*11*) have shown that elements and compounds that wet graphite (that is, with surface tensions of ≤190 mN/m) are potential candidates for nanotube-filling materials. More recently, a simple wet chemical method was developed for the opening and filling of nanotubes, which facilitates the inclusion of a wide variety of materials (*14*). The tubes are treated with diluted nitric acid in which a metal salt is dissolved; once a tube has been opened, the liquid enters the nanotube, and the formation of enclosed metal oxide particles can be induced by a subsequent calcinating step. A drawback of this method is that initially the nanotube is filled mostly with the solvent.

To resolve this and other problems, we have developed a four-step procedure involving: (i) synthesis of the tubes, (ii) opening, (iii) high-temperature annealing, and (iv) capillary filling with a molten pure metal salt such as $AgNO_3$ (*15*). It was verified that in the case of $AgNO_3$, the molten salt entered the tubes. In some cases, the tubes were filled along their entire length (*16*). Metallization of the encapsulated salt was induced by the electron beam in an electron microscope, which was used to monitor the chemical reactions inside the tube. The results presented here illustrate several processes occurring in the nanotube cavities, namely: (i) the filling process (capillarity and wetting), (ii) the metallization (decomposition of silver nitrate and silver bead formation), and (iii) chemical reactions between evolved gases and the nanotube interior.

The filling efficiency (~2 to 3%) is much lower than the efficiency to open tube tips by oxidation (~60%), resulting in only a small fraction of the opened tubes being filled. The inner diameter distribution of the nanotubes peaks at ~2 nm (Fig. 1A), but the filled tube cavities are usually those with a large inner diameter (≥4 nm), and filling of small diameter tubes (1 to 2 nm) was not observed (Fig. 1B). The low percentage of filled nanotubes thus simply reflects the low abundance of large inner diameter tubes, the majority of which were filled. Similar filling diameters were also observed by others using various

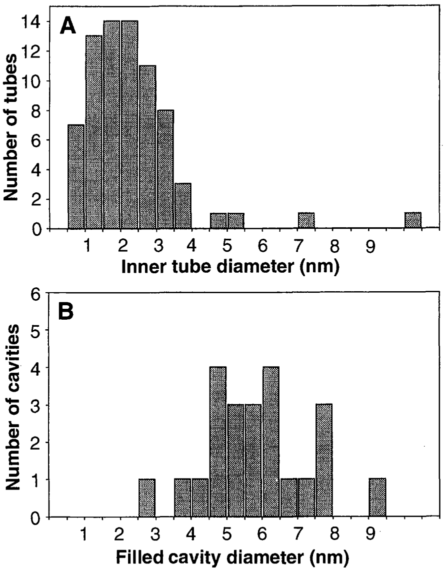

Fig. 1. (**A**) Histogram of the diameter distribution of the inner cavity of arc-generated multilayered carbon nanotubes (74 tubes); (**B**) Inner diameter distribution of filled nanotubes (26 tubes).

D. Ugarte, Laboratório Nacional de Luz Síncrotron (CNPq/MCT), Caixa Postal 6192, 13083-970 Campinas SP, Brazil.
A. Châtelain, Institut de Physique Expérimentale, Département Physique, Ecole Polytechnique Fédérale de Lausanne, 1015 Lausanne, Switzerland.
W. A. de Heer, School of Physics, Georgia Institute of Technology, Atlanta, GA 30332, USA.

*To whom correspondence should be addressed. E-mail: ugarte@LNLS.BR

experimental approaches (*11, 12, 14, 17*) [with the exception of lead compounds and vanadium oxides (*12, 18*), for which filling of tubes with ≈1 nm diameter has been reported]. Hence there is a size constraint on the capillary filling of nanotubes. It appears that the capillarity of narrow tubes (1 to 2 nm or less) is reduced and that wetting depends on the cavity size (*19*). In contrast, previous treatments of nanotube capillarity followed a size-independent approach based on bulk-like liquid-graphite interfaces (*11*).

Wetting and hence capillary filling occurs when the liquid-solid contact angle $\theta_c < 90°$ (*11, 20*). θ_c is related to the liquid surface tension γ by $\cos \theta_c = (\gamma_{SV} - \gamma_{SL})\,\gamma^{-1}$, where γ_{SV} and γ_{SL} are the surface tensions at the solid-vapor and solid-liquid interfaces, respectively. If there is no chemical bonding nor charge transfer, the solid-liquid interaction may be assumed to be dominated by van der Waals forces and can be expressed in terms of dielectric polarizabilities (*20*), giving $\cos \theta_c = 2\,(\alpha_S/\alpha_L) - 1$, where α_S and α_L are the polarizabilities of the solid and liquid, respectively. The polarizability of the vapor is neglected (*20*). Given these approximations, the wetting condition becomes $\alpha_L < 2\,\alpha_S$. The neglected interactions are important, for example, in the case of lead carbonate filling of nanotubes (*12*) and when charge is transferred to the cages as observed for metal atoms in narrow tubes (*21, 22*) and in metallofullerenes (*23*). However, our salt-graphite system is simpler and should be approximated reasonably well by the polarizability model. This approximation allows us to identify and to estimate size effects, for example the occurrence of a wetting to non-wetting transition if the polarizabilities depend on the cavity diameter.

The polarizabilities of bulk graphite and silver nitrate were estimated by using the Clausius-Mossotti expression (*24*), and the dielectric constants (ε) were obtained from the corresponding refraction index. For graphite, an anisotropic material, we consider the case of the electric field perpendicular to the graphene layer, resulting in $\varepsilon_{\text{gra}} = 1.8$; for silver nitrate we obtain $\varepsilon_{\text{AgNO}_3} = 3.0625$. With these values we obtain $\theta_c \approx 86°$, which is quite close to the critical angle (90°), indicating that even small changes in the polarizabilities will affect the wetting conditions.

We next show that the polarizability of a concave graphite surface (for example, the nanotube interior) is reduced compared with planar graphite. As remarked by Haddon (*25*), fullerene chemistry relates directly to the strain on the graphitic network. The strain is expressed in terms of the pyramidalization angle defined as $\theta_P = (\theta_{\sigma\pi} - 90°)$, where $\theta_{\sigma\pi}$ is the angle between the σ and π orbitals of a bent sp^2-like bond. Deviations from planarity cause the hybridization to become intermediate between sp^2 (that is, graphite, $\theta_P = 0°$) and sp^3 (that is, diamond, $\theta_P = 19°$). In this process, π electron density shifts from the concave surface to the convex surface (*25, 26*). Consequently, the chemical activity of the concave side is reduced as a result of the reduced local density of states at the Fermi level, and the chemical activity of the convex side is increased. Related effects are known for nonplanar organic molecules, for which significant changes in chemical reactivities have been observed for $\theta_P = 6°$ to 7° (*25, 27*). The reduced local density of states at the Fermi level of the concave surface also causes a reduction in the polarizability. Curvature-induced bonding changes in nanotubes have previously been characterized by electron energy loss spectroscopy (*28*). Within experimental limits (0.7-eV energy resolution), no differences were found between graphite and multiwalled nanotubes (5 to 20 nm in diameter); for single-walled nanotubes (*29, 30*) (≈1 nm in diameter), the π^* band showed no modifications, but important changes were observed for the σ^* fine structure.

For nanotubes with inner diameters of 1.5 to 2 nm (the most abundant ones in our sample), θ_P is about 5°, in the range where hybridization shifts are known to be important (*25, 27*), so that we may conclude that the nonfilling of the narrow tubes is caused by this size effect. Moreover, considering that the critical diameter for filling is 4 nm ($\theta_P \approx 2°$) and using the polarizability of bulk silver nitrate, we can estimate the polarizability from a 4-nm nanotube cavity by $\alpha_S = \alpha_{\text{AgNO}_3}/2$.

If we assume that the wetting can be described purely in terms of the polarizabilities (α_S and α_L), and that the polarizability of the filling material does not change with decreasing size (*31*), the wetting (and filling) of any dielectric material can be predicted once the curvature dependence of the graphitic polarizability is known. To the lowest order of approximation, the cavity polarizability (α_{cav}) may be considered to depend linearly on θ_P (which is a simple function of the radius of curvature), so that we may write $\alpha_{\text{cav}}(\theta_P) = \alpha_{\text{gr}}\,(1 - 0.0275\,\theta_P)$, where α_{gr} is the polarizability of planar graphite, and θ_P is measured in degrees. This approach allows us to predict the filling properties of other materials; for example, in the case of vanadium pentoxide (taking the dielectric constant as $\varepsilon_{\text{V}_2\text{O}_5} \approx 2.25$), we find that the wetting threshold occurs for a cavity diameter of ≈7 Å ($\theta_P \approx 11.5°$), in agreement with experimental observations (*18*).

Note that the narrow inner diameter distribution of multilayer nanotubes (1.5 to 2 nm on average, Fig. 1A) is very close to the diameter distribution of single-layer nanotubes generated in arc discharges with transition metal–carbon electrodes (1.2 to 2 nm on average) (*29, 30*). This result suggests a common formation mechanism in the production of single- and multilayer tubes. The transition metal dopant may in fact inhibit multi-layer growth, rather than catalyze single-layer growth as is often assumed. Moreover, as in the formation of carbon onions, we suspect that temperature is probably the parameter that defines the average inner-tube size (*32*).

Silver nitrate decomposes under the electron microscope beam, leading to the forma-

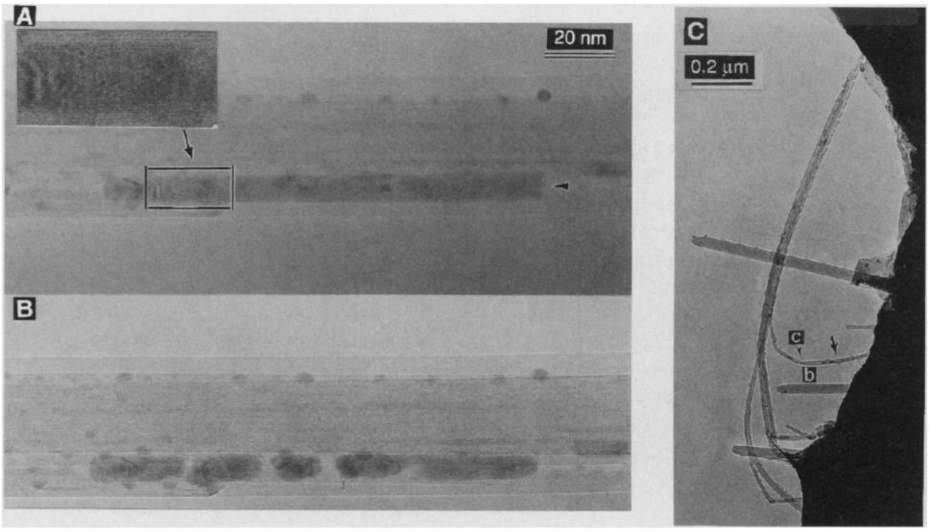

Fig. 2. (**A**) A silver nitrate filament enclosed in a nanotube cavity. The lattice fringes perpendicular to the tube axis correspond to the (220) planes of silver nitrate ($d_{220} = 2.53$ Å). (**B**) After a few minutes of in situ electron irradiation, metallization of the filament was induced, leading to the formation of a chain of metallic silver beads. (**C**) Low magnification micrograph of graphitic nanotubes filled with chains of silver particles produced by prolonged irradiation of silver nitrate–filled nanotubes (10 min, dose ≈1 A/cm^2). The beaded filling pattern continues over the entire length of the nanotubes.

tion of pure silver particles (Fig. 2); this decomposition of silver nitrate is expected to be closely related to the thermolysis of this salt: $2AgNO_3 \rightarrow 2Ag + 2\ NO_2 + O_2$. Initially, continuous dark filling of a tube (7 nm in diameter and 120 nm in length) is observed (Fig. 2A). On the right-hand side, a region filled with low contrast material has a concave meniscus (marked with an arrow), which indicates that the molten salt wets the nanotube cavity. The material on the left-hand side of the same filament (which has been partially reduced by the electron beam) clearly has a convex meniscus, that is the material in this region does not wet the cavity. Hence, this micrograph captured the particle during its transformation from silver nitrate to pure silver. Prolonged electron irradiation yields a discontinuous metallic filling formed by a series of elongated particles (Fig. 2B). A low magnification electron micrograph after prolonged irradiation (Fig. 2C) illustrates that this pattern is observed along the entire length of the nanotubes (0.5 to 1 μm), indicating that before metallization, the molten salt must have filled the tubes over their entire length.

The metallic particles filling the nanotubes (Fig. 3) display an aspect ratio of about 3 and consist of one or several domains; several of them present either (111) or (200) silver lattice fringes. These particles fit tightly in the nanotube, and the tube is intact at the tube-particle interface. However, the tube walls between the metal particles are markedly thinner (Fig. 3B) because of the erosion of the innermost nanotube layers (four to six shells) by the corrosive gases liberated in the decomposition of $AgNO_3$. Qualitatively, the level of erosion can be estimated from the granular contrast inside the tube, because this granularity almost certainly results from the amorphous carbon debris from the reaction (no granularity is observed in empty tubes). In region a (Fig. 3A), the granular structure is much more dense than in region b. These contrast variations can easily be explained by noting that the nanotube cavity region a is bounded on either end by a silver bead separated by $\sim$10 nm, so that the evolved gases remain trapped there at high pressures, causing the decomposition of the walls. On the other hand, the nanotube cavity region b is $\sim$100 nm long (see region marked b in Fig. 2C, which also corresponds to b in Fig. 3), and therefore the oxidizing gas pressure is much reduced compared to a, leading to less destruction of the walls. Moreover, note that in Fig. 2C, region b is particularly bright compared to neighboring parts of the cavity, probably because the oxidizing gases leaked out before causing substantial damage to the walls. This observation could indicate that gases punctured the tube at the sharp bend in region c because of preferential oxidation of strained graphitic regions. Related effects have been observed, for example, in the higher reactivities of pentagons in fullerenes and in nanotube tips (*11, 13, 14*).

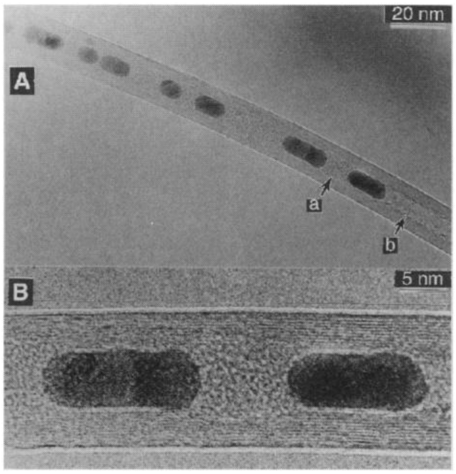

Fig. 3. (**A**) High-resolution electron micrograph of a nanotube densely filled with silver particles. (**B**) Detailed view of the silver beads in the lower right of (A) showing the eroded inner layers of the nanotube.

The pressures inside the tube may become extremely high. In region a (Fig. 3), for example, if we assume that the cavity reflects a 26% reduction in volume occupied by the solid after the reaction, the evolved gases would exert a pressure of about 1300 bar (at room temperature). The possibility to produce high-pressure phases encapsulated in nanotubes has already been suggested (*12*). Here we have provided evidence for a reaction resulting in high-pressure trapped gases in a nanotube.

REFERENCES AND NOTES

1. H. W. Kroto, J. R. Heath, S. C. O'Brien, R. F. Curl, R. E. Smalley, *Nature* **318**, 162 (1985).
2. S. Iijima, *ibid.* **354**, 56 (1991).
3. R. S. Ruoff, D. C. Lorents, B. Chan, R. Malhotra, S. Subramoney, *Science* **259**, 346 (1993).
4. D. Ugarte, *Chem. Phys. Lett.* **209**, 99 (1993).
5. M. Tomita, Y. Saito, T. Hayashi, *Jpn. J. Appl. Phys.* **32**, L280 (1993).
6. S. Seraphin, D. Zhou, J. Jiao, J. C. Withers, R. Loutfy, *Nature* **362**, 503 (1993).
7. P. Ajayan *et al.*, *Phys. Rev. Lett.* **72**, 1722 (1994).
8. C. Guerret-Plécourt, Y. Le Bouar, A. Loiseau, H. Pascard, *Nature* **372**, 761 (1994).
9. T. W. Ebbesen and P. M. Ajayan, *ibid.* **358**, 220 (1992).
10. M. R. Pederson and J. Q. Broughton, *Phys. Rev. Lett.* **69**, 2689 (1992).
11. E. Dujardin, T. W. Ebbesen, H. Hiura, K. Tanigaki, *Science* **265**, 1850 (1994).
12. P. M. Ajayan and S. Iijima, *Nature* **361**, 333 (1993).
13. P. M. Ajayan *et al.*, *ibid.* **362**, 522 (1993).
14. S. C. Tsang, Y. K. Chen, P. J. F. Harris, M. L. H. Green, *ibid.* **372**, 159 (1994).
15. The nanotubes were produced with the dc arc-discharge method (20 V, 70 to 90 A) with graphite electrodes of 6 mm in diameter in a 350-mbar He atmosphere. As usual, the nanotubes were found in the soft sooty fibrous core material that was encapsulated in a hard-shelled cylindrical deposit on the cathode. The core material was ultrasonically dispersed in ethanol, dried, and then oxidized in air, first for 10 min at 550°C and subsequently for 10 min at 650°C, whereby about 60% of the tubes were opened. This process usually leaves some amorphous carbonaceous material at the tip (*13*). This material was removed by annealing the sample for 30 min at 2000°C. The high-temperature treatment graphitizes the amorphous material (which may otherwise plug the tube) and also removes dangling bonds left by the oxidation procedure. The sample was thoroughly mixed with silver nitrate, and the resulting powder was then heated to 230°C for 30 min (that is, slightly above the melting point of silver nitrate at 212°C). The purity and evolution of the sample were analyzed after each step of the procedure with a transmission electron microscope (Philips EM 430 ST).
16. Electron microscopy studies were performed on samples prepared by crushing the solidified silver nitrate deposit (containing nanotubes) after the heat treatment; in consequence, the tubes were often partially embedded in large salt particles (see Fig. 2). Our attempts to remove the excess silver nitrate enrobing the tubes by dissolving it in an ultrasound bath of distilled water were unsuccessful. This treatment caused the material inside the tubes to be removed as well.
17. R. M. Lago, S. C. Tsang, K. L. Lu, Y. K. Chen, M. L. H. Green, *J. Chem. Soc. Chem. Commun.* **1995**, 1355 (1995).
18. P. M. Ajayan, O. Stephan, P. Redlich, C. Colliex, *Nature* **375**, 564 (1995).
19. It is possible that the narrow tubes are closed. Even though the high-temperature annealing of nanotubes opened by oxidation removes the amorphous carbon material at the opened end (*13*), the annealing could conceivably close the tubes again in a process that could be more efficient for narrower tubes. This closure could remain undetected by electron microscopy. However, in experiments with molten metals or wet chemical techniques, the typical diameters of the material filling the tubes were also $\sim$5 nm (*11, 14, 17*). This result is relevant because in these cases the narrower tubes were certainly open.
20. P. G. de Gennes, *Rev. Mod. Phys.* **57**, 827 (1985).
21. Y. Miyamoto, A. Rubio, X. Blase, M. L. Cohen, S. G. Louie, *Phys. Rev. Lett.* **74**, 2993 (1995).
22. A. Rubio, Y. Miyamoto, X. Blase, M. L. Cohen, S. G. Louie, *Phys. Rev. B* **53**, 4023 (1996).
23. K. Laasonen, W. Andreoni, M. Parrinello, *Science* **258**, 1916 (1992).
24. J. D. Jackson, *Classical Electrodynamics* (Wiley, New York, 1967).
25. R. C. Haddon, *Science* **261**, 1545 (1993).
26. K. Henke and H. Hopf, *Angew. Chem. Int. Ed. Engl.* **15**, 165 (1976).
27. X. Blase, L. X. Benedict, E. L. Shirley, S. G. Louie, *Phys. Rev. Lett.* **72**, 1878 (1994).
28. O. Stéphan, P. M. Ajayan, C. Colliex, *Phys. Rev. B* **53**, 13824 (1996).
29. S. Iijima and T. Ichihashi, *Nature* **363**, 603 (1993).
30. D. S. Bethune *et al.*, *ibid.* **363**, 605 (1993).
31. We assume that the polarizability of the filling material is similar to that of the bulk. This approximation is reasonable for the metal and the salt, because for metallic particles of these sizes deviations are $<1\%$ [W. A. de Heer, *Rev. Mod. Phys.* **65**, 611 (1993)], and for the salt we expect even smaller deviations because of the very short range of the electrostatic forces. In contrast, polarizability deviations for the graphitic systems are much more important because of the highly directional nature of covalent bonds. We have, however, ignored nanotribological and nanoviscous effects, which could affect the filling rates. These properties are now under further investigation.
32. W. A. de Heer and D. Ugarte, *Chem. Phys. Lett.* **207**, 480 (1993).
33. We acknowledge stimulating discussions and valuable suggestions from Dr. P. M. Ajayan. The electron microscopy studies were performed at the Centre Interdépartamental de Microscopie Electronique (CIME), Ecole Polytechnique Fédérale de Lausanne. We are indebted to the Brazilian Council for Scientific and Technologic Research (CNPq) and the Swiss National Science Foundation for financial support.

31 July 1996; accepted 25 October 1996